

Design analysis of ductile failure in dovetail connections

Tomohiro Naruse, 3rd Department, Mechanical Engineering Research Laboratory, Hitachi, Ltd., Japan

Dr. Donald Mackenzie, Department of Mechanical Engineering, University of Strathclyde, Scotland, UK.

Abstract

The static plastic collapse of ductile dovetail structures is investigated by three analysis methods: slip line field (SLF) theory based on a sheet drawing model, finite element limit analysis and linear elastic finite element analysis with adapted pressure vessel design stress linearization and categorisation methods. A range of angles and heights are considered in the investigation. Three experimental test cases are also presented. The limit analysis results are found to give the best comparison with the limited experimental results, indicating similar collapse loads and modes of ductile collapse. The SLF solution is found to give conservative but useful failure loads for low dovetail angles but at angles greater than 30°, the solution is not generally conservative. The pressure vessel design by analysis stress categorization procedure was adapted for dovetail analysis and was found to give reasonably conservative collapse loads in most cases. However, the procedure requires the designer to consider number of different stress classification lines to ensure that a conservative collapse load is identified. It is concluded that the finite element limit analysis approach provides the best and most direct route to calculating the allowable

load for the joint and is the preferred method when appropriate finite element analysis facilities are available.

1. Introduction

Dovetail joints are used to connect components in many kinds of rotary machines, such as the rotor rim and core in the hydroelectric motor-generator illustrated in Fig. 1. When such an assembly rotates, the dovetail structure locks the rotating components together. Strength evaluation of the dovetail structure is a fundamental consideration in rotor design. Two types of failure mode are considered when designing rotating dovetail configurations: fatigue failure due to cyclic loading (for example, start-stop operating conditions) and gross plastic collapse under static load (for example, single application of excessive angular acceleration). Recently, finite element analysis (FEA) has been applied to detailed fatigue assessments of dovetail structures [1-9]. Papanikos *et al.* [2] and Burguete *et al.* [3] compared the results of FEA with those of photoelastic results, Sinclair *et al.* [4-5] investigated the influence of friction and proposed a numerical model, and others have concentrated specifically on contact stress and fretting fatigue [6-9]. However, to date FEA has not been used to assess the gross plastic collapse mechanism. It has been standard practice in dovetail joint design to base the static strength assessment on the calculated nominal stress at the neck (section C-C' in Fig. 1) and comparison with similar existing designs. However, depending on the joint geometry, static plastic collapse does not always occur across the neck.

The tensile test arrangement shown in Fig. 2 was used to investigate the failure of three model dovetails milled and ground from ductile steel plate. The dovetail angle was

($\alpha=$) 30° and heights were ($h_1=$) (a) 25 mm, (b) 34 mm and (c) 60 mm. The failed specimens shown in Fig. 3 each exhibit a different form of plastic rupture. The smallest specimen (a) failed by gross plastic deformation of the shoulders of the specimen and was pulled through the mating mandrill without breaking. The middle-sized specimen (b) experienced gross plastic deformation in both shoulders of the joint and eventual failure by ductile tearing at an angle of approximately 55° to the neck in one shoulder of the dovetail. The largest specimen (c) failed by gross plastic deformation and eventual ductile tearing across the neck of the specimen. Safe design against static failure of dovetail joints requires a design methodology that identifies the appropriate form of failure and calculates the corresponding plastic failure load. In this paper, three approaches to modelling plastic collapse of the dovetail are considered. Two are based on pressure vessel Design by Analysis (DBA) procedures and the third on Slip Line Field (SLF) theory.

Gross plastic deformation is a fundamental failure mechanism considered in pressure vessel design. The ASME Boiler and Pressure Vessel Code Section VIII Division 2 [10], PD5500 [11] and EN13445 [12] provide DBA procedures on preventing plastic collapse. These procedures are based on both elastic and inelastic stress analysis. No specific analysis methods are specified in the codes but in recent years FEA has become the most commonly used, although the elastic design rules in particular are clearly related to concepts in thin shell analysis. In the elastic analysis procedure, the total elastic stress is

categorized into three classes of stress, *primary*, *secondary* and *peak* stress. Gross plastic deformation is precluded by limiting the primary stress with respect to a specified design stress. In the inelastic analysis procedures, gross plastic deformation is prevented by restricting the allowable load with respect to either the *limit load* or the *plastic load* of the vessel. The *limit load* is the maximum load satisfying equilibrium between external loads and internal forces when an elastic-perfectly plastic material model and small deformation theory are assumed. The *plastic load* is calculated by a more complex analysis, in which large deformation effects and/or material strain hardening are included and a criterion of plastic collapse is applied. The Slip Line Field (SLF) method can be used to solve for stress and velocity fields in the plastic collapse state when assuming a rigid-perfectly plastic solid and plane strain conditions [12]. The governing equation of plane plastic flow is hyperbolic and can be solved by applying the method of characteristics and SLF matrix-operator methods [13]. In the present investigation, allowable loads calculated by DBA elastic stress analysis, limit analysis and SLF theory results were compared for a range of dovetail geometries.

2. Analysis of Plastic Collapse

Model dovetail joints similar to the specimens described in Figs. 2 and 3 were investigated. Five dovetail angles, $\alpha=10^\circ, 30^\circ, 35^\circ, 40^\circ,$ and 50° , were considered. Five dovetail heights were used for each angle: $h_1=25, 29, 34, 45, 60$ mm. The joint

dimensions are defined in Fig. 4 and Table 1, (dovetail dimensions lower case mating die upper case). The height, H_3 , the width, W_2 , and the thickness of the female die are considerably larger than the dimensions of the dovetail, such that the female die behaves like a semi-rigid structure. The joint reduction ratio, r , is also tabulated in Table 1, where

$$r = 1 - \frac{h}{H} = \frac{2 \sin \alpha}{1 + 2 \sin \alpha}, \quad (1)$$

where $2h$ is the width of neck as shown in Fig. 5, which corresponds with w_4 as shown in Fig. 4, and $2H$ is the width of dovetail as shown in Fig. 5, which corresponds with w_5 as shown in Fig. 4. The models' material properties were Young's modulus $E=207$ GPa, yield stress $\sigma_Y = 784$ MPa, design stress intensity $S_m=522.7$ MPa (defined as the allowable stress of primary membrane stress [10], with a value of approximately $2/3\sigma_Y$ for most pressure vessel steels) and Poisson's ratio $\nu=0.3$. All FE analysis was performed using the ANSYS v.10 program.

2.1 Slip line field solution

The slip-line field shown in Fig. 5 [14] is for sheet extrusion or drawing through a frictionless wedge-shaped die of angle α . This configuration is similar to the dovetail problem. The main difference is that the length of material on the entrance side of the die is finite in the dovetail model but infinite in the sheet drawing model. This SLF solution was investigated as a possible analysis model for dovetail designs [14-17]. Slip-line

fields for sheet drawing change with the reduction r and can be derived as shown in Fig.

6. The slip line field shown in Fig. 6 (a) is now called Type I, which is valid for a reduction $r \leq 2\sin\alpha / (1+2\sin\alpha)$. Angles α , θ and ψ are related by the expression

$$\psi = \theta + \alpha . \quad (2)$$

The drawing force cannot be derived directly because the hydrostatic pressures p_B and p_D on points B and D respectively are unknown. The sum of forces in a horizontal direction across OBE, $\Sigma Fx'_{OBE}$, can be written in terms of p_B as,

$$\sum Fx'_{OBE} = kFx_{BE} \cos(\angle B) - kFy_{BE} \sin(\angle B) + k\overline{OB} \cos(\angle B) - p_B H \quad (3)$$

where \overline{OB} is the length of line OB, $\angle B$ is the angle of point in an anticlockwise sense, such that $\angle B = -\alpha - \theta - \pi/4$, and Fx_{BE} and Fy_{BE} are the force components acting on slip-line BE at the base point B, assuming hydrostatic pressure to be zero. Slip-line field can be solved theoretically in some special cases such as $\psi=0$ in Fig. 6 (a). The matrix-operator method is applied to solve for the force components Fx_{BE} and Fy_{BE} [14].

Constant k is obtained from the yield criterion assuming plane strain conditions:

$$\frac{1}{4}(\sigma_x - \sigma_y)^2 + \tau_{xy}^2 = k^2 , \quad (4)$$

and has value $k = \sigma_Y/2$ for the Tresca criterion or $k = \sigma_Y/\sqrt{3}$ for the von Mises criterion.

The hydrostatic pressure p_B can be evaluated by equating the sum of forces in the horizontal direction across OBE to zero, as there is no net force on the drawn sheet. The total force in the horizontal direction across ADE can similarly be written as

$$\sum Fx'_{ADE} = kFx_{DE} \cos(\angle D) - kFy_{DE} \sin(\angle D) + k\overline{AD} \cos(\angle D) + p_D H \quad (5)$$

where \overline{AD} is the length of line AD and $\angle D = -\alpha + \psi - 3\pi/4$ is the angle of point D.

Fx_{DE} and Fy_{DE} are the force components acting on slip line DE at the base point D,

assuming hydrostatic pressure to be zero, and are obtained by using the matrix-operator

method. The hydrostatic pressure p_D remains unknown, but p_D and p_E can be determined

from the Hencky equations

$$\begin{aligned} p + 2k\phi &= \text{constant} \quad \text{on an } \alpha \text{- line and} \\ p - 2k\phi &= \text{constant} \quad \text{on a } \beta \text{- line.} \end{aligned} \quad (6)$$

Such that

$$\begin{aligned} p_E &= p_B - 2k\psi \\ p_D &= p_E + 2k\theta. \end{aligned} \quad (7)$$

Thus the drawing force, $\Sigma Fx'_{ADE}$, can be calculated.

The slip line field shown in Fig. 6 (b) is termed Type II, which is valid for $r > 2\sin\alpha /$

$(1+2\sin\alpha)$ and $0 < \eta < \alpha$. The total forces in the horizontal direction across HGED,

$\Sigma Fx'_{HGED}$, can be written as,

$$\begin{aligned} \sum Fx'_{HGED} &= kFx_{DE} \cos(\angle D) - kFy_{DE} \sin(\angle D) + kFx_{GH} \cos(\angle G) - kFy_{GH} \sin(\angle G) \\ &\quad + k\overline{EG} \cos(\angle G) + p_D H_E + p_E (H - H_E) \end{aligned} \quad (8)$$

where

$$\angle D = \frac{3}{4}\pi - \alpha + \eta \quad \text{and} \quad \angle G = \frac{3}{4}\pi. \quad (9)$$

Fx_{DE} , Fy_{DE} , Fx_{GH} and Fy_{GH} are the force components acting on slip-lines DE and GH,

assuming hydrostatic pressure to be zero, and can be evaluated by using the matrix-operator method. p_D and p_E are hydrostatic pressures. From the Hencky equations (6),

$$p_D = p_E + 2k(\alpha - \eta). \quad (10)$$

The hydrostatic pressures p_D and p_E can be evaluated by equating the total force $\Sigma Fx'_{HGED}$ to zero, as there is no net force on the drawn sheet, thus:

$$\begin{aligned} p_C &= p_D - 2k\eta \\ p_B &= p_C - 2k\eta. \end{aligned} \quad (11)$$

Then the drawing force $\Sigma Fx'_{OB}$, which expresses the total force in the horizontal direction across OB, is calculated as

$$\Sigma Fx'_{OB} = k\overline{OB} \cos(\angle B) + p_B h \quad (12)$$

2.2 Limit analysis

Classical limit analysis is based on an idealised rigid-perfectly plastic or elastic-perfectly plastic material model and small deformation theory. However, in this analysis, an elastic-perfectly plastic material model with large deformation theory is assumed, (to better represent the contact condition between the dovetail and the female die), therefore the analysis is not strictly speaking a limit analysis. The analysis utilises the Newton-Raphson iterative solution algorithm, in which the solution progresses in a step-wise manner until convergence or termination due to violation of equilibrium

between internal and external forces. The limit load is defined here as the load giving the final convergent solution before an unconverged termination.

The ANSYS plasticity routines are based on the von Mises yield criterion. EN13445 [12]

Annex B (the direct route) *B.8.2 Gross Plastic Deformation (GPD) B.8.2.1 Principle*

specifies that the “Von Mises' yield condition may be used instead of Tresca's, but then the design strength parameter shall be multiplied by $\sqrt{3}/2$.” This procedure is followed here.

A typical FE model of the assembly is shown in Fig. 7. A half model is analyzed and symmetry boundary condition applied. The bottom line of the female die is fixed in the vertical direction. A pulling force is applied at the centre of the upper line of the dovetail.

The vertical degrees of freedom on the upper line of the dovetail are coupled to the vertical displacement of the loaded node. The dovetail material is elastic-perfectly plastic.

The female die is elastic. A frictionless contact condition is applied between the dovetail and the die. The dovetail thickness is small enough to be considered to be a thin plate, thus plane stress elements with specified thickness are used in both the dovetail and die.

This plane stress assumption contradicts the slip-line field approach, in which plane strain conditions are assumed.

2.3 Elastic analysis and stress categorization

Pressure vessel DBA based on elastic stress analysis requires the designer to partition or categorise the elastic stress field into three different classes of stress: *primary*, *secondary*

and *peak* stress. Primary stress is an equilibrium stress field associated with gross plastic deformation. Secondary stress arises from compatibility equilibriums and, when taken in conjunction with primary stress, is associated with incremental plastic collapse under cyclic operating loads. Peak stress is a locally concentrated stress and, when taken in conjunction with primary plus secondary stress, is associated with fatigue failure. The pressure vessel codes consider the primary and secondary stresses to have constant membrane or linear bending through-wall distributions, in accordance with the concepts of thin shell theory. Gross plastic deformation is precluded by limiting the allowable value of primary membrane stress and primary membrane plus bending stress with respect to the design stress S_m of the material.

Many pressurised components do not behave like thin shell structures, in that the stress distribution through the component is not linear: i.e. does not comprise of membrane and bending distributions. This is also the case for dovetail structures. In order to apply the DBA procedures to such components, it is common practice to evaluate a linearised stress distribution that has the same global (membrane and bending) effect on the component as the actual non-linear distribution. This procedure is called stress linearization and the section on which stress is linearised is called the stress classification line (SCL). In stress linearization, the through-thickness distribution of each of the six elementary stresses, σ_{ij} , along the SCL are linearised into membrane and bending components. The linearised stresses are then used to evaluate the stress intensity

or equivalent stress distributions along the SCL, for comparison with the Tresca or von Mises yield criteria respectively. Stress intensity S_{INT} is calculated from principal stresses σ_1 , σ_2 and σ_3 as:

$$S_{INT} = \max(|\sigma_1 - \sigma_2|, |\sigma_2 - \sigma_3|, |\sigma_3 - \sigma_1|). \quad (13)$$

Equivalent stress S_{EQV} is given by:

$$S_{EQV} = \sqrt{\frac{(\sigma_1 - \sigma_2)^2 + (\sigma_2 - \sigma_3)^2 + (\sigma_3 - \sigma_1)^2}{2}}. \quad (14)$$

The ASME Code [10] requires the use of the Tresca criterion and stress intensity in DBA calculations. However, EN13445 [12] Annex C (method based on stress categories) permits use of an equivalent stress based on either the Tresca or von Mises criterion. The latter will be used in the stress categorisation results presented here.

The ANSYS program includes a stress linearization postprocessor that calculates the linearised component stresses, stress intensity and equivalent stress distributions along an SCL specified by the designer. These decomposed stresses are classified into five different categories of stress: general primary membrane stress (P_m), local primary membrane stress (P_L), primary bending stress (P_b), secondary stress (Q) and peak stress (F).

Individual or collected classified stresses are compared with the different allowable values, so as to design against specific failure mechanisms. It is essential that the decomposed stress is correctly classified because their allowable values differ. The Codes provide explicit classification guidance for some typical pressure vessel

geometries and load conditions. In the analysis of ductile failure of a dovetail under static loading, the stress categories of interest are primary membrane and primary membrane plus bending stress.

The FE models used in the limit analysis, as defined in Fig. 7 and Table 1, were also used for stress linearization and classification. Elastic material properties were used throughout and a fixed pulling force equivalent to 400 MPa of nominal stress in the neck applied. In elastic analysis, it is not possible to determine the limiting SCL a priori and a range of values for the SCL angle γ were considered, as illustrated in Fig. 8 (a). Only the SCL with $\gamma=0$ conforms to the definition of SCL used in pressure vessel design, as it extends unbroken across the neck of the dovetail. For $\gamma \neq 0$, the SCL is effectively a “V” shape about the plane of symmetry or effectively bisects the shoulder of the dovetail.

Applying the linearization procedure gives values for membrane and bending stress along each SCL considered. These are then categorized and the appropriate stress limit applied to define the allowable load. Stress categorization for the dovetail configuration is not covered explicitly in pressure vessel codes and here classification was defined by considering the basic definition of primary stress. The membrane stress is classified as *general primary membrane* stress, because no redistribution of load occurs if the membrane stress exceeds yield. The allowable value for primary membrane stress intensity is S_m . The bending stress was classified by considering a limiting case of the dovetail design, which is the “T” tail structure shown in Fig. 8 (b). The “T” structure can

be considered as two cantilevers joined at the plane of symmetry. The bending stress in the cantilever components is required to maintain equilibrium with the external pulling force and is therefore designated as *primary bending* stress. The allowable value for primary membrane plus bending stress intensity is $1.5S_m$.

3. Results

The calculated collapse loads and angles given by the SLF analysis, limit analysis and stress categorisation analysis for the range of joints considered are given in Table 2.

In TYPE I SLF analysis, the angle θ was varied within $0^\circ \leq \theta \leq 90^\circ - \alpha$. In TYPE II the angle η was varied within $0^\circ \leq \eta \leq \alpha$. The relationship between the reduction ratio r and drawing force normalized by $2k$ is shown in Fig. 9. The normalised drawing force $p/2k$ increases with reduction ratio r and the die angle α . In a uniaxial solution, plastic collapse occurs across the neck section of the dovetail (width, $2h$ in Fig. 5 (b)) when the stress on this plane reaches yield: that is $p/2k=1.0$. The SLF solution shows that the normalised drawing force is less than the uniaxial collapse load for relatively small reduction ratios, r , indicating that plastic collapse occurs at a slip-line in the dovetail before the neck yields.

The limit analysis (von Mises) equivalent plastic strain distributions at the final converged results for a dovetail with die angle ($\alpha=$) 30° and heights ($h=$)25, 34, 60 mm

are shown in Figs. 10 (a) to (c) respectively. In each model, a region of high plastic strain has formed at the point of contact between the dovetail and die at the neck and spreads along an approximately straight line to form the plastic failure surface. When the dovetail height is relatively small (i.e. the reduction ratio is small) as in Fig. 10 (a), the collapse line terminates at the bottom surface of the dovetail, indicating failure within the shoulders of the joint: the shoulders are sheared off. When the reduction ratio is large, as in Fig. 10 (c), the dovetail fails on the horizontal plane across the neck of the dovetail. For an intermediate value of reduction ratio, as in Fig. 10 (b), the collapse line extends from the surface to the plane of symmetry, giving a V-shaped plastic failure surface. The collapse angle, γ , is defined in Fig. 10. If the collapse line lies on the neck of the dovetail, as in Fig. 10 (c), the collapse angle is $\gamma=0^\circ$.

Values for the normalised limit load given by the limit analysis are compared with the SLF curves in Fig. 11. The FEA limit load results, based on the von Mises criterion, have been modified by multiplying by $\sqrt{3}/2$, as discussed in Section 2.2. There is a fundamental difference in the state of stress assumed in these analyses: the SLF solution assumes plane strain, the limit analysis plane stress. It is seen that the calculated limit load and SLF drawing force are similar for die angles of $\alpha=10^\circ$ and 30° . However, a significant difference between the solutions is seen for larger die angles, in which the limit load is lower than the SLF drawing force. By interpolating, the limit analysis drawing force is found to achieve a maximum value at about $\alpha=35^\circ$. The SLF drawing

force continues to rise with increasing die angle. In some configurations, the SLF load is significantly larger than the limit load until the $p/2k$ cut-off is reached. This indicates that the SLF solution is not generally conservative.

The limit and slip line collapse angles for two dovetails with $\alpha=30^\circ$ and $h_1=25$ mm, $\alpha=30^\circ$ and $h_1=34$ mm, are shown in Figs. 12 (a) and (b) respectively. Points A to E and O are points on a Type I SLF, as defined in Fig. 6 (a). The limit load collapse surface of the shorter joint clearly corresponds to slip line AE in Fig. 12 (b). Thus the collapse angle, γ , obtained by limit analysis is almost equal to the angle of $\angle PAD$. However, for the shorter dovetail shown in Fig. 12 (a) no such clear correlation is found. Limit load collapse in this case occurs on a plane that lies between slip lines AE and AB. Comparing the limit and SLF results, the SLF analysis precisely predicts the limit load for dovetails with die angles smaller than 30° . When the die angle is larger than 30° , the failure load predicted by SLF analysis is larger than the limit load. It is therefore not conservative to calculate the allowable load for such dovetails by SLF analysis.

Fig. 13 shows the von Mises equivalent stress contour plot for a dovetail with $\alpha=30^\circ$ and $h_1=34$ mm given by elastic analysis. A range of stress classification lines are considered. These lines originate from the edge at the point of contact with the die with varying angle, γ , with respect to the horizontal. The constituents of plane stress, σ_x , σ_y and τ_{xy} , are represented in the local coordinate system on the SCL. Fig. 14 shows the maximum equivalent membrane stress and equivalent membrane plus bending stress

evaluated in the model shown in Fig. 13 for a range of classification lines with $0^\circ \leq \gamma \leq 90^\circ$. The linearised stresses are normalized with respect to the nominal normal stress in the neck of the dovetail, w_4 in Fig. 4. The membrane and membrane plus bending equivalent stresses are seen to vary significantly with the angle of the stress classification line. This was found to be true for all the joints considered in the study. In general, the SCL angle giving the highest stress varies inversely with dovetail height, h_1 . The calculated plastic load of the dovetail joint is determined by the maximum membrane or membrane plus bending stress; therefore it is dependent on the angle of the SCL. Failure loads based on membrane and membrane plus bending stress can be evaluated from the applied load by proportionality. Both the membrane stress and membrane plus bending stress are compared to their allowable values for each SCL considered. As the DBA procedures include a nominal design factor of 1.5 against plastic collapse, collapse loads are obtained by factoring the allowable stress by 1.5. It is found that the SCL across the minimum cross section, or neck, of the dovetail does not generally give a conservative value of plastic load. The variation of predicted plastic collapse line shows some similar behaviour to the collapse lines given by limit analysis.

The elastic analysis/stress categorisation plastic collapse loads are compared with the SLF drawing force in Fig. 15 and Table 2. Good agreement is seen for the smallest taper angle of 10° , but in all other cases the stress categorisation load is markedly lower than

the SLF solution. Comparison with the limit load results, as shown in Table 2, shows that the collapse load predicted by stress linearization (based on the von Mises criterion) is similar to the limit load (von Mises criterion factored by $\sqrt{3}/2$) for the 10° models. The predicted collapse load was less than the limit load for all other geometries except two models that had a high reduction ratio and 50° die angle. In these cases, the results of limit analysis predicted failure across the neck of the joint, w_1 in Fig. 4. The linearization and categorisation investigation considered only SCLs starting at the point of contact and in these cases predicted failure horizontally across the dovetail from this point, w_4 in Fig. 4. In general, the failure load predicted by stress linearization is much smaller than the limit load for the reduction ratio range from 0.5 to 0.8. The angle of the critical SCL in the stress linearization analyses was found to be similar to the collapse angle predicted by limit analysis for many configurations but was not consistent over the range considered

4. Comparison with test results

The measured failure load and collapse angle for the three 30° dovetails shown in Fig. 2 are given in Table 3, together with the results of the corresponding analyses. Good agreement is found between the measured and analysis collapse loads for the shortest dovetail, with reduction ratio $r=0.305$. The limit analysis collapse angle is similar to the measured collapse plane but the collapse angle given by the stress categorisation

procedure is significantly different, at about half the value. In the intermediate dovetail, $r=0.470$, the calculated collapse loads are conservative with respect to the experimental load. Limit analysis gives the highest analytical load, followed by the SLF and stress categorisation loads. The limit collapse angle is similar to the measured test angle but the stress categorisation plane is again significantly different. In the longest dovetail, $r=0.691$, the limit and stress categorisation collapse loads are conservative with respect to the measured load. The normalised SLF load is not conservative with a value of 1.209. However, this value does not take account of the $p/2k=1$ truncation of the SLF curves corresponding to failure in the neck, which should be applied when the SLF value exceeds 1. As before, the limit collapse angle is similar to the test angle but the stress categorisation angle differs significantly.

5. Conclusions

Three analysis methods for determining the static plastic collapse loads for dovetail structures were investigated: SLF theory based on a sheet drawing model, finite element limit analysis and linear elastic finite element analysis with stress categorization. All three methods were found to give similar results for a dovetail angle of 10° . However, the calculated failure loads were found to differ for larger dovetail angles.

The incremental elastic plastic finite element analysis method used in the limit analysis

calculations is the most representative method used and the one that shows greatest similarity with the limited experimental results available. The method requires the designer to have knowledge and experience of inelastic FEA, which may limit applicability of the method. However, it has the advantage that it simulates the plastic failure mechanism and gives a direct evaluation of allowable load (hence the name direct route in EN13445). Limit analysis showed three collapse modes, which turned from *line collapse* to *V-shaped collapse* and finally to *neck collapse*, with increasing reduction ratio. The limit load of dovetails with similar reduction ratios has an optimum value when the die angle is around 35°.

The SLF solution requires no additional specialist knowledge from the designer and can be used to generate design data in a variety of forms. This approach was found to give acceptable conservative failure loads for the 10° and 30° dovetails considered. However, at angles greater than 30°, the SLF solution may give values for collapse loads that are too high.

Stress categorization procedure of pressure vessel design by analysis was adapted for dovetail analysis and was found to give reasonable conservative collapse loads in most cases. Although this requires use of elastic FEA only, which is simpler and easier for the designer to perform than inelastic FEA, the categorisation procedure is time consuming. The plastic failure surface in the dovetail may vary from a plane straight across the neck of the joint to shearing of the shoulders of the joint at 90° to this plane. It is necessary to

investigate a number of SCLs to determine which plane between 0° and 90° gives the lowest collapse load and hence determines the allowable design load. This requires repetitive application of the stress linearization procedures for a number of lines at different angles, however, the method is conservative and may be appropriate in some design environments.

As only three test results are available it is not possible to generalise on the relationship between the analysis and test results. In the three particular cases, the limit analysis approach showed good correspondence with the tests for both failure load and failure plane angle. The stress categorisation and SLF methods also gave conservative collapse loads.

The choice of method used in design depends on the staff and facilities available and the form of the dovetail joint. The SLF method is suitable for small angle dovetail joint design but may not be conservative for angles greater than 30°. The stress categorisation method gives conservative values of collapse loads and is generally suitable for design. However, it is a time-consuming approach because the designer must consider a number of SCLs to ensure the worst case is identified. Limit analysis requires inelastic finite element analysis but gives the most complete simulation of the plastic failure mechanism. Furthermore, the calculated limit loads provide the best and most direct route to calculating the allowable load for the joint.

References

- 1 Meguid, S. A., Refaat, M. H. and Papanikos, P.** Theoretical and Experimental Studies of Structural Integrity of Dovetail Joints in Aeroengine Disc. *Journal of Materials Processing Technology*, 1996, **56**, 668—667.
- 2 Papanikos, P., Meguid, S. A. and Stjepanovic, Z.** Three-dimensional nonlinear finite element analysis of dovetail joints in aeroengine discs. *Finite Elements in Analysis and Design* **29**(1998), 173—186.
- 3 Burguete, R. L. and Patterson, E. A.** Comparison of numerical and experimental analyses for contact problems under normal and tangential loads. *Proceeding Institution Mechanical Engineers* 215(2001), 113—123.
- 4 Sinclair, G. B., Cormier, N. G. and Griffin, J. H.** Contact Stress in Dovetail Attachments: Finite Element Modeling. *Journal of Engineering for Gas Turbines and Power*, 2002, **124**, 182—189.
- 5 Sinclair, G. B. and Cormier, N. G.** Contact Stress in Dovetail Attachments: Physical Modeling. *Journal of Engineering for Gas Turbines and Power*, 2002, **124**, 325—331.
- 6 Papanikos, P. and Meguid, S. A.** Theoretical and Experimental Studies of Fretting-Initiated Fatigue Failure of Aeroengine Compressor Discs. *Fatigue & Fracture of Engineering Materials & Structures*, 1994, **17**, 539—550.

- 7 Ruiz, C., Boddington, P. H. B. and Chen, K. C.** An investigation of fatigue and fretting in a dovetail joint. *Experimental Mechanics*, 1984, **24**(3), 208—217.
- 8 He, M. J. and Ruiz, C.** Fatigue life of dovetail joints: verification of simple biaxial model. *Experimental Mechanics*, 1989, **29**(2), 126—131.
- 9 Conner, B. P. and Nicholas, T.** Using Dovetail Fixture to Study Fretting Fatigue and Fretting Palliatives, *Journal of Engineering Materials and Technology* , 2006, **128**, 133—141.
- 10 ASME.** Boiler and Pressure Vessel Code, 2003 (ASME, New York).
- 11 BSI.** PD5500: Unfired Fusion Welded Pressure Vessels, 1999 (British Standards Institution, London).
- 12 CES.** EN 23445-3:2002 Unfired pressure vessels, 2002 (European Committee for Standardisation, Brussels).
- 13 Calladine, C. R.** Plasticity for engineers, 1985 (Ellis Horwood limited).
- 14 Johnson, W., Sowerby, R. and Venter, R. D.** Plane strain slip line fields for metal deformation processes a source book and bibliography, 1982 (Pergamon Press).
- 15 Kitagawa H.,** Basis of plasticity (in Japanese), 1992 (Nikkankougyoushinbun).
- 16 Ewing, D. J. F.** A series method for constructing slip-line fields. *Journal of Mechanics and Physics of Solids*, 1968, **15**, 105.

17 Dewhurst, P. and Collins, I. A matrix technique for constructing slip-line field solutions to a class of plane strain plasticity problems. *International Journal of Numerical Methods in Engineering*, 1973, **7**, 357.

Table 1 Dimensions of dovetail models

Die angle	Dimension of dovetail				Dimension of female	Reduction ratio
	w_2	(w_4)	(w_5)	h_1		
10°	25.8	20.12	23.73	25	41.2	0.1521
	27.1	20.12	25.03	29	41.2	0.1961
	28.7	20.12	26.63	34	41.2	0.2444
	32.2	20.12	30.13	45	41.2	0.3322
	37.4	20.12	35.33	60	41.2	0.4305
30°	39	21.07	30.34	25	90	0.3055
	43	21.07	34.34	29	90	0.3864
	48.4	21.07	39.74	34	90	0.4698
	60	21.07	51.34	45	90	0.5896
	76.8	21.07	68.14	60	90	0.6908
35°	43	21.45	31.98	25	105.2	0.3294
	48	21.45	36.98	29	105.2	0.4201
	54.4	21.45	43.38	34	105.2	0.5056
	68.5	21.45	57.48	45	105.2	0.6269
	89.1	21.45	78.08	60	105.2	0.7253
40°	46.8	21.87	33.02	25	122.2	0.3375
	53.5	21.87	39.72	29	122.2	0.4493
	61.4	21.87	47.62	34	122.2	0.5407
	78.2	21.87	64.42	45	122.2	0.6605
	102.7	21.87	88.92	60	122.2	0.7540
50°	58	22.86	36.95	25	165.4	0.3814
	67.6	22.86	46.55	29	165.4	0.5090
	78.7	22.86	57.65	34	165.4	0.6035
	102.7	22.86	81.65	45	165.4	0.7201
	137.5	22.86	116.45	60	165.4	0.8037

Table 2 Prediction of limit loads and collapse angles according to stress categorization

Dimension of dovetail			SLF	Limit Analysis		Stress Categorisation	
Die angle	Dovetail height	Reduction ratio	Drawing force	Limit load	Limit Collapse angle	Collapse load	Collapse angle
α	h_1	r	$p/2k$	$p/2k$	γ	$p/2k$	γ
10°	25	0.152	0.206	0.223	40.0	0.208	43.8
	29	0.196	0.241	0.256	42.6	0.245	45.6
	34	0.244	0.289	0.307	47.2	0.303	47.8
	45	0.332	-	0.431	52.1	0.430	48.4
	60	0.430	-	0.626	54.6	0.555	31.2
30°	25	0.305	0.537	0.516	61.7	0.495	33.7
	29	0.386	0.619	0.642	61.0	0.547	30.9
	34	0.470	0.721	0.783	43.7	0.626	29.8
	45	0.590	0.927	1.018	44.3	0.743	26.6
	60	0.691	1.209	1.024	0.0	0.830	23.3
35°	25	0.329	0.610	0.560	61.6	0.544	76.9
	29	0.420	0.708	0.692	63.6	0.614	36.2
	34	0.506	0.819	0.852	57.7	0.695	33.8
	45	0.627	1.044	1.011	0.0	0.808	33.6
	60	0.725	1.339	1.009	0.0	0.890	34.4
40°	25	0.338	0.666	0.568	71.1	0.548	77.4
	29	0.449	0.795	0.721	76.5	0.649	40.1
	34	0.541	0.922	0.902	69.2	0.737	40.3
	45	0.660	1.178	1.001	0.0	0.863	39.2
	60	0.754	1.467	1.001	0.0	0.961	24.9
50°	25	0.381	0.769	0.592	82.3	0.586	75.6
	29	0.509	0.979	0.749	73.9	0.736	48.7
	34	0.604	1.131	0.947	72.1	0.836	48.9
	45	0.720	1.413	0.963	0.0	0.992	47.1
	60	0.804	1.740	0.963	0.0	1.076	0.0

Table 3 Comparison of experimental results and analyses results

h_l (mm) (r)	Exp. collapse Load $p/2k$	SLF Drawing Force $p/2k$	Limit Load $p/2k$	Stress cat. Collapse Load $p/2k$	Exp. Collapse angle ($^\circ$)	Limit collapse angle ($^\circ$)	Stress cat. Collapse angle ($^\circ$)
25 (0.305)	0.565	0.537	0.516	0.495	65	62	34
34 (0.470)	0.938	0.721	0.783	0.626	45	44	30
60 (0.691)	1.080	1.209 (1.000)*	1.024	0.83	0.0	0	23

* $p/2k=1$ truncation

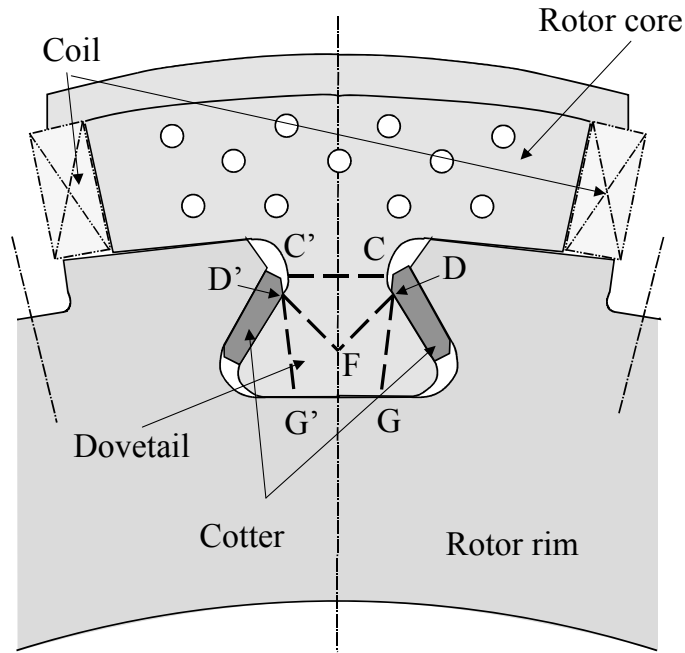


Fig. 1 Dovetail structure of hydroelectric motor generator

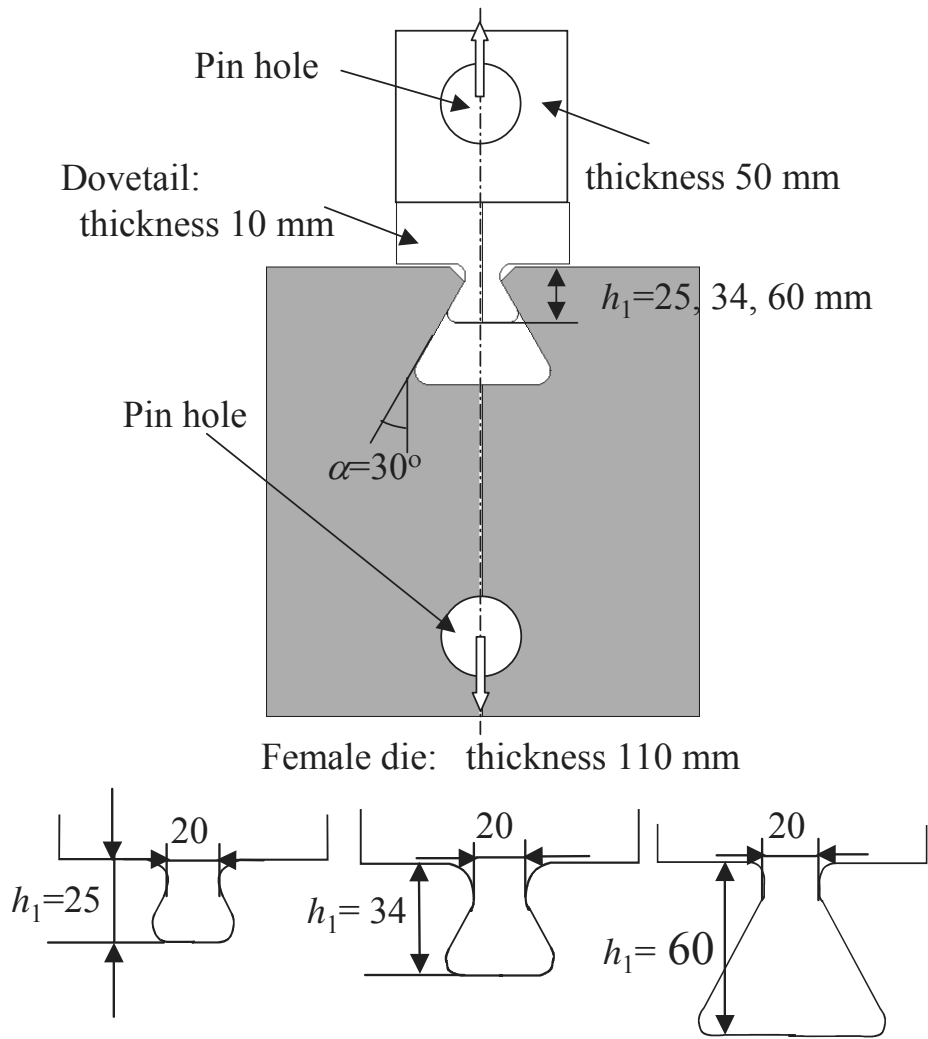


Fig. 2 Three dovetail specimens

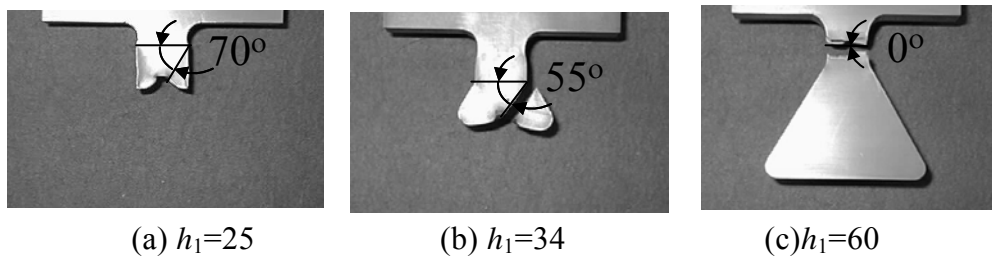


Fig. 3 Collapse modes of three dovetail specimens

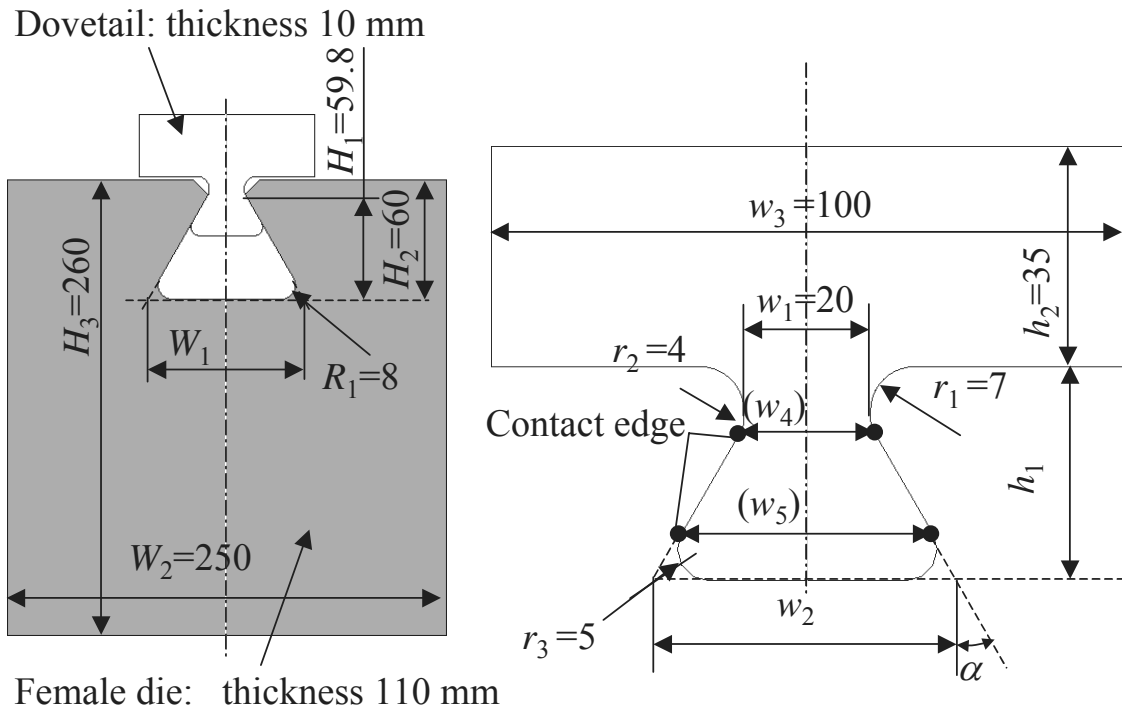
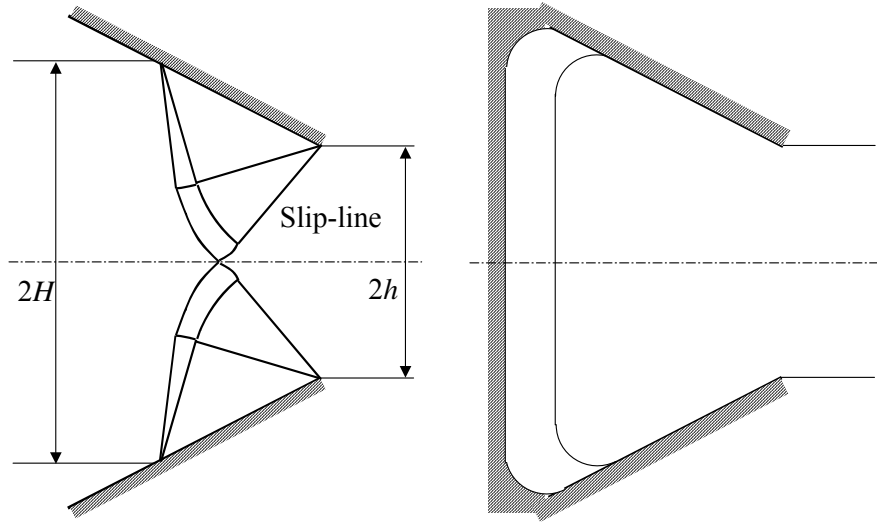
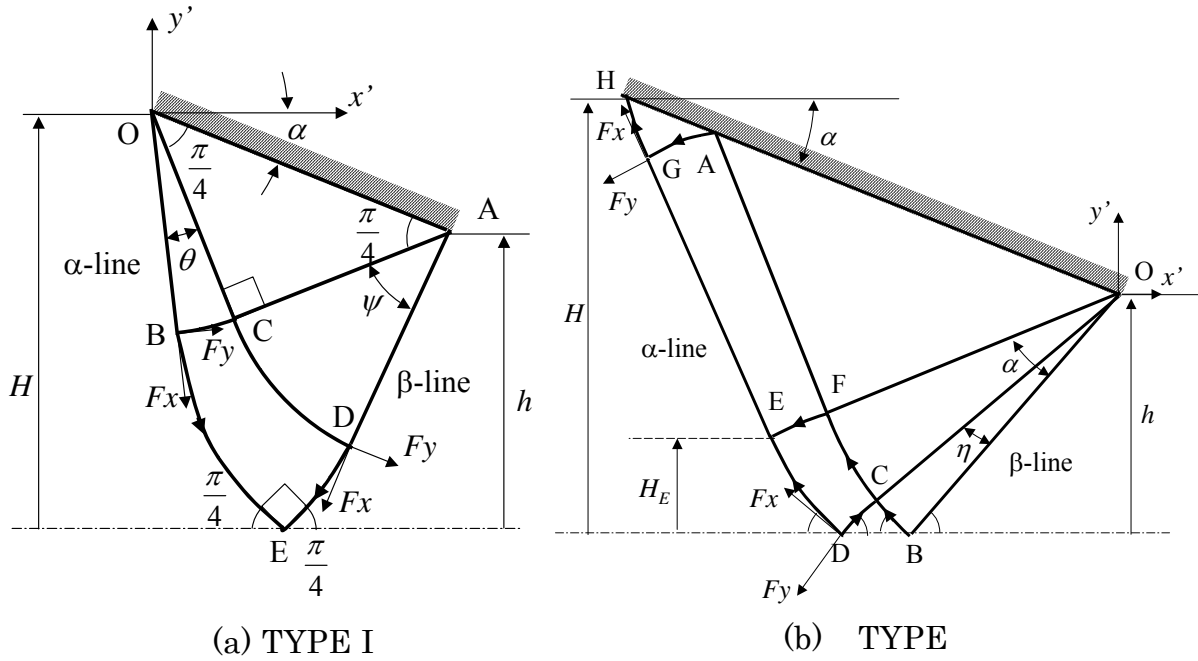


Fig. 4 Dimensions of dovetail models



(a) Slip-line of sheet drawing (b) Dovetail structure

Fig. 5 Slip-line of sheet drawing and dovetail structure



(a) TYPE I

(b) TYPE

Fig. 6 Slip-line field of drawing sheet

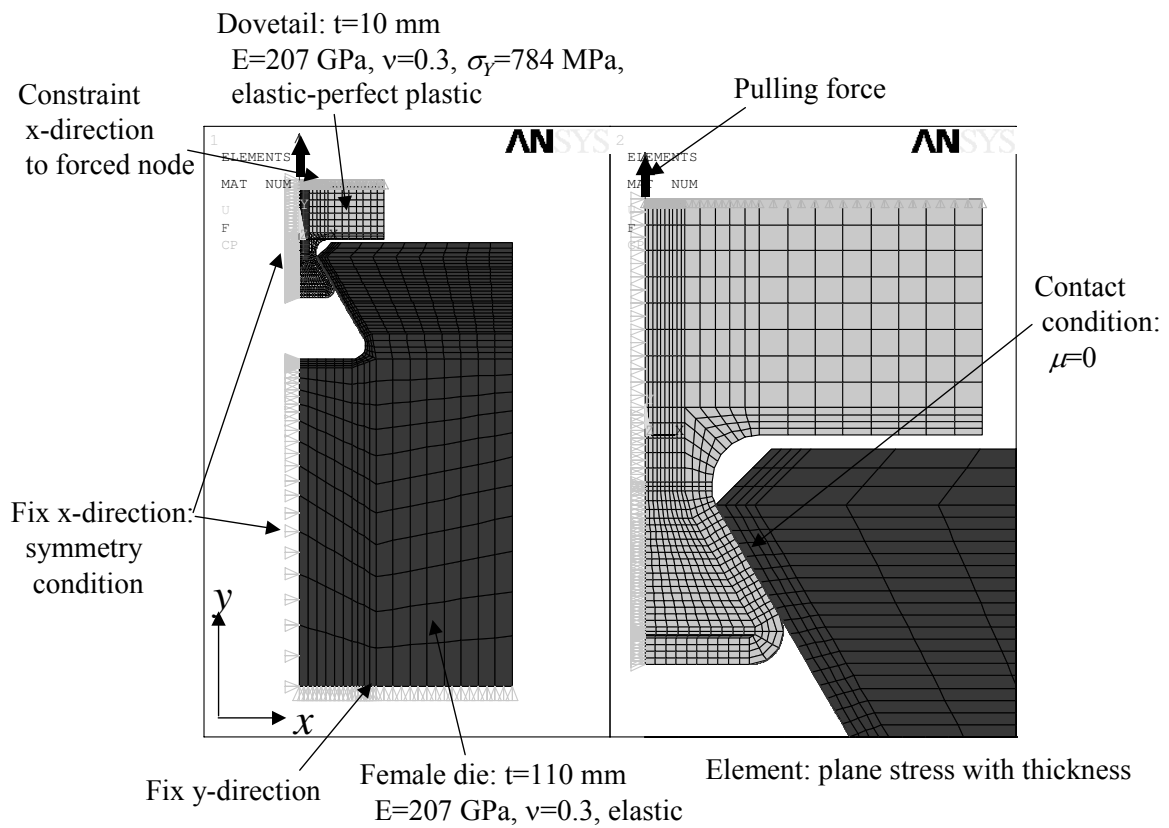


Fig. 7 FE model of dovetail

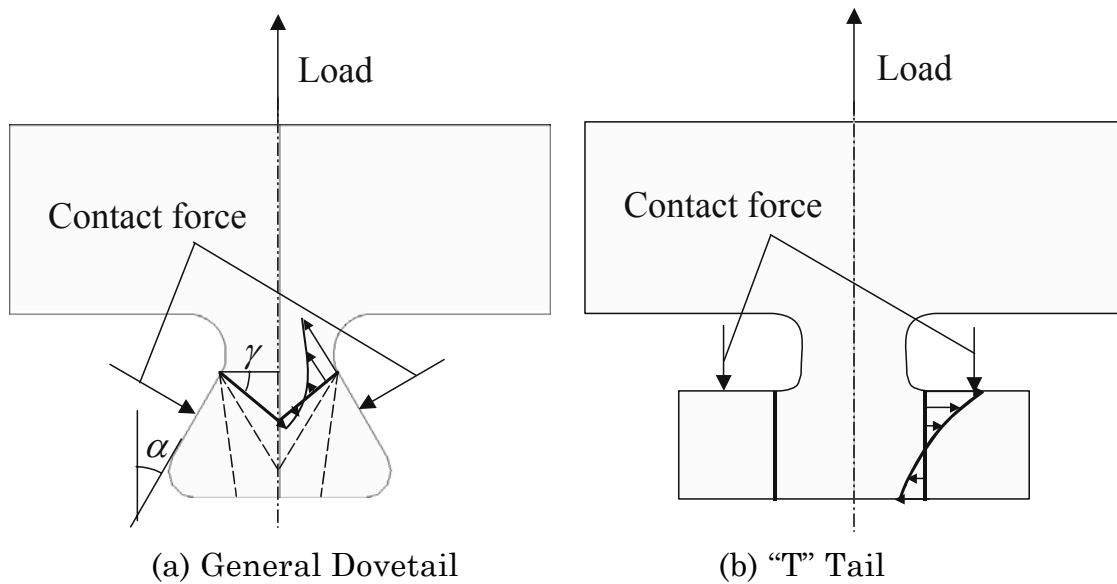


Fig. 8 Supported line segments of dovetail structure

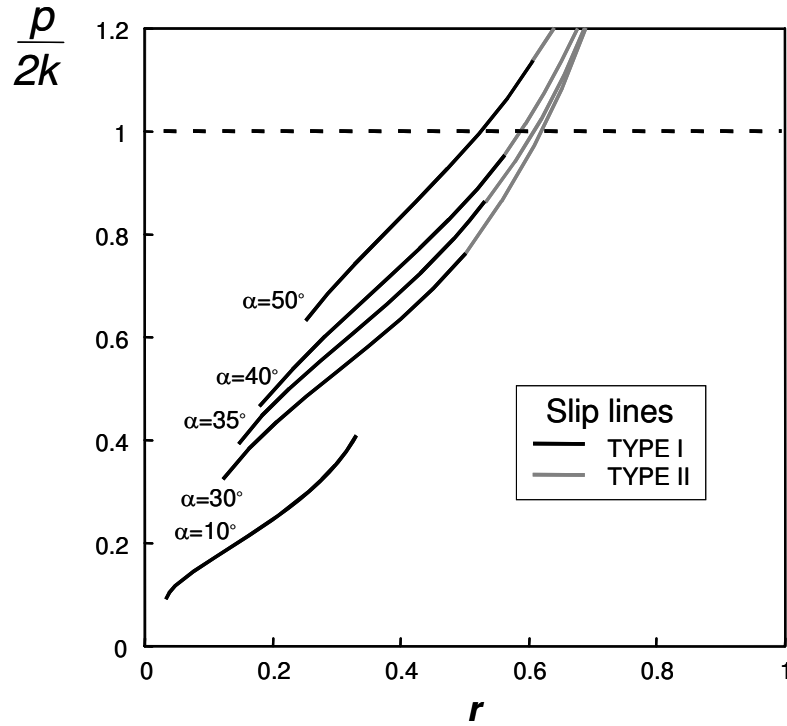
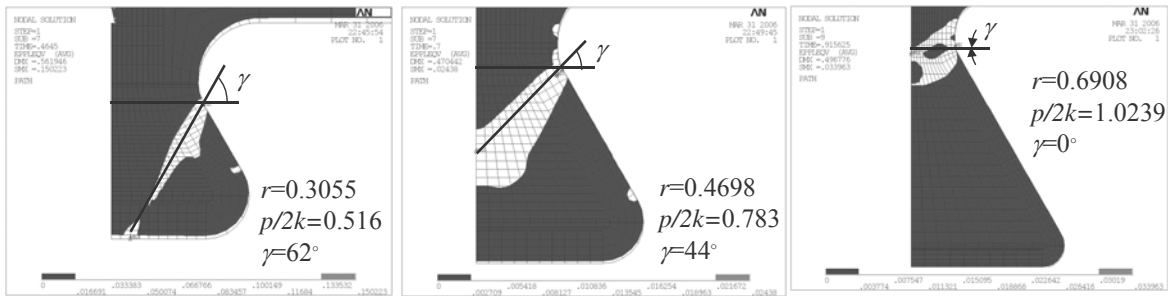


Fig. 9. SLF solution for relation between reduction ratio and drawing force of slip-line field



(a) $h=25$ mm

(b) $h=34$ mm

(c) $h=60$ mm

Fig. 10 Contour of total equivalent strain with die angle $\alpha=30^\circ$

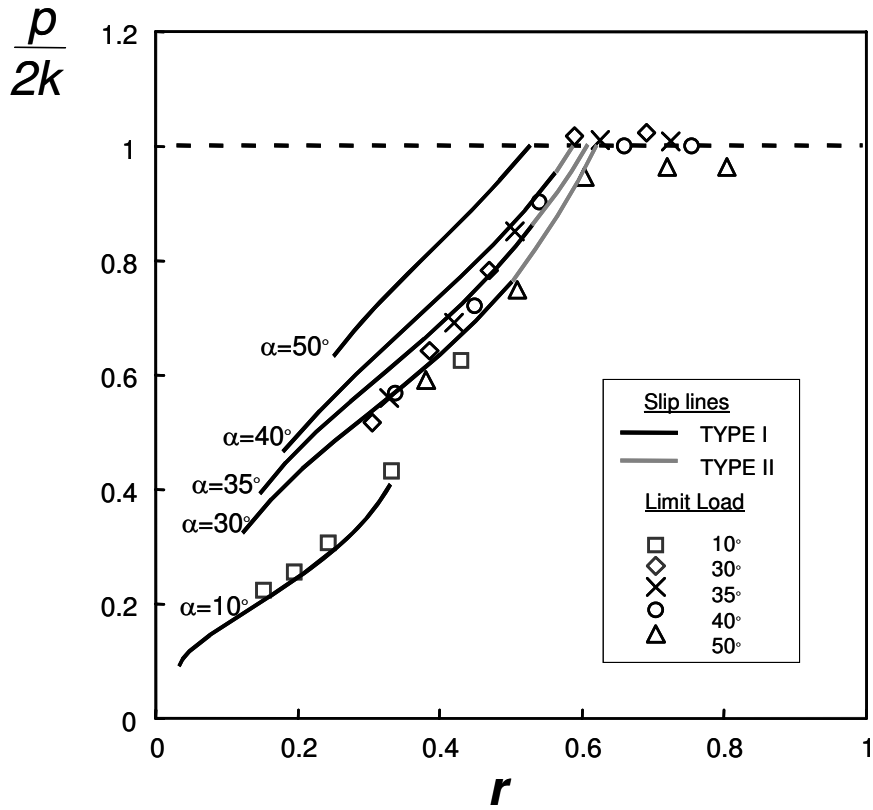
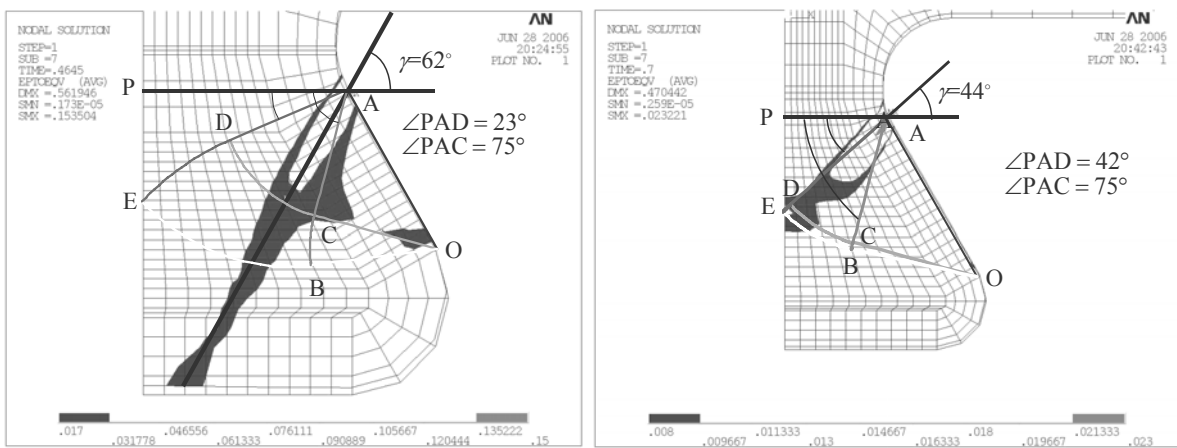


Fig. 11 Relation between reduction ratio and drawing force of slip-line field and limit analysis



(a) $\alpha=30^\circ, h_1=25 \text{ mm}$

(b) $\alpha=30^\circ, h_1=34 \text{ mm}$

Fig. 12 Comparison between collapse line of limit load and slip-line field

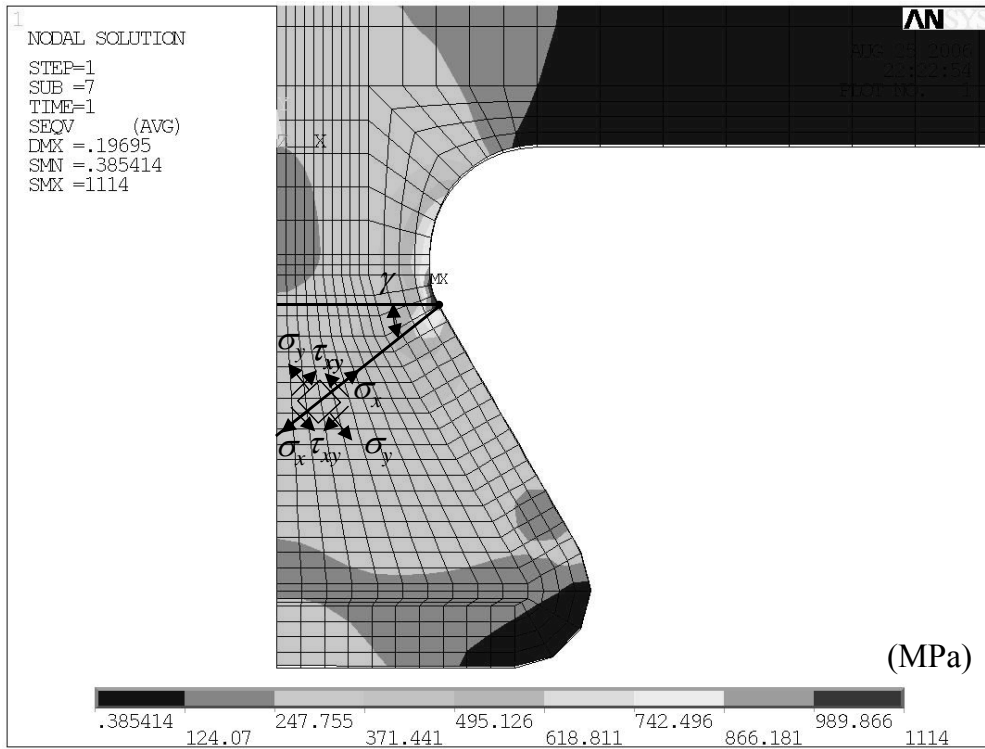


Fig. 13 Contour of equivalent stress with $\alpha=30^\circ$, $h_1=34$ mm

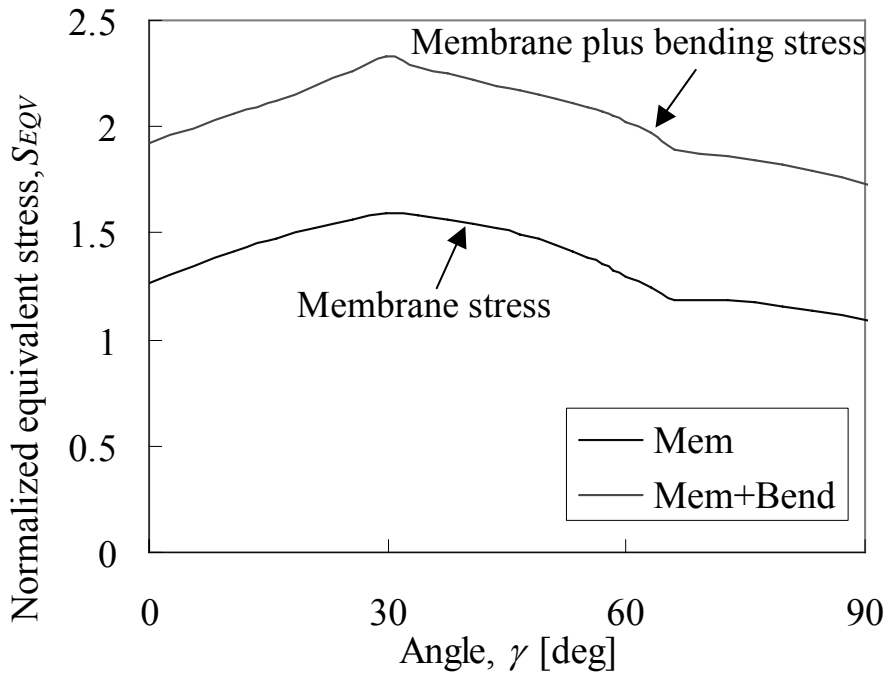


Fig. 14 Relation between angle of stress classification line, γ , and equivalent stress, S_{EQV} , with $\alpha=30^\circ$, $h_1=34$ mm

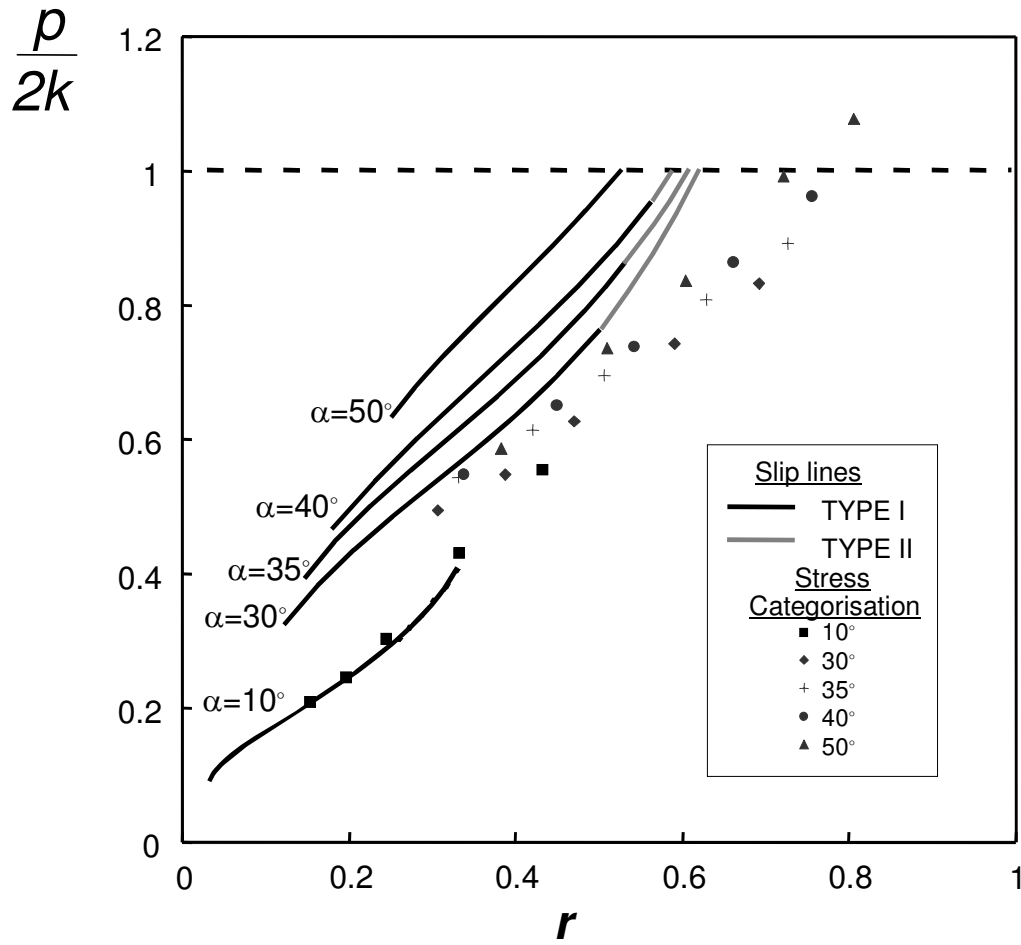


Fig. 15 Relation between reduction ratio and drawing force of slip-line field and stress categorization